ISSN 1070-3632, Russian Journal of General Chemistry, 2021, Vol. 91, No. 5, pp. 897–903. © Pleiades Publishing, Ltd., 2021.

Syntheses, Characterization, and Luminescence Properties of Three Coordination Complexes with Sulfonate-Phenol Anions and Trivalent Metal Ions

Pengpeng Yin[a], Chang Liu[a], Ying Wang[a], Lei Guan[a,*], Xian Chen[a], Xuejia Xiong[a], and Hongzhe Jin[a]

[a] *School of Petrochemical Engineering, Liaoning Petrochemical University, Fushun, 113001 China*
**e-mail: coord_gl@163.com*

Received January 21, 2021; revised February 11, 2021; accepted May 5, 2021

Abstract—A dinuclear Tb complex, $Tb_2(H_2L)_3(phen)_2$ (**1**), and two similar N-donor coordination complexes, $Fe(phen)_3 \cdot HL$ (**2**), $Fe(bipy)_3 \cdot HL \cdot 5H_2O$ (**3**) (Na_2H_2L = 4,5-dihydroxy-1,3-benzenedisulfonic acid disodium salt, phen = 1,10-phenanthroline and bipy = 2,2′-bipyridine), have been synthesized and characterized by single crystal X-ray diffraction and elemental analyses. Complex **1** features a phenoxo-O bridged Tb dinuclear structure, in which the dinuclear Tb^{3+} ions reside in distorted double-capped triangular prism and dodecahedral coordination environments, respectively. Introduction of phen and bipy moieties contributes to formation of low dimensional dinuclear structure. Complexes **2** and **3** feature similar N-donor mononuclear structures, where HL^{3-} anions remain uncoordinated with protonated phenol groups, respectively. Complex **1** exhibits the characteristic emission peaks of Tb^{3+} ion, and the luminescent properties of complexes **2** and **3** can be attributed to the intraligand transitions.

Keywords: Luminescence property, coordination complex, dinuclear, Tb^{3+} ion

DOI: 10.1134/S1070363221050200

INTRODUCTION

Recently, dinuclear and multinuclear coordination complexes received close attention because of their remarkable properties in catalysis, adsorption, molecular sieving, fluorescence, and single-molecule magnets [1–6]. Polyfunctional ligands are usually empolyed to generate dinuclear and multinuclear coordination complexes with various architectures in the bridging modes [7–9]. To date, a broad number of dinuclear and multinuclear discrete complexes based on bridging ligands have reported in [10–12]. Rational design and assembly still remain a challenge in constructing novel topologies of dinuclear complexes, targeting the structure–properties correlations [13–15]. Dinuclear structures depend on the geometries and functional groups of the organic ligands. A significant effort has been directed towards modification of organic ligands by different functional groups, such as carboxylate, phenol and sulfonate, and controlling self-assembly of the desired structures [16–18]. To our best knowledge, phenol oxygen atoms of organic ligands can efficiently bridge metal ions building stable dinuclear structures making it easy for the ligands containing the phenol groups to form dinuclear complexes with intricate structures.

Herein, we report the syntheses, characterization and properties of one dinuclear coordination complex with brdiging H_2L^{2-} ligands, $Tb_2(H_2L)_3(phen)_2$, and two similar N-donor coordination complexes, $Fe(phen)_3 \cdot HL$ and $Fe(bipy)_3 \cdot HL \cdot 5H_2O$. The TG and fluorescence properties of complexes **1**–**3** have been studied.

RESULTS AND DISCUSSION

Crystal structure of $Tb_2(H_2L)_3(phen)_2$ (1). The complex **1** is characterized by dinuclear structure, and it crystallizes in the triclinic space group *P*-1 (Table 1). The asymmetric unit contains two Tb ions, three H_2L^{2-} ligands

Scheme 1. Structure of the Na_2H_2L ligand.

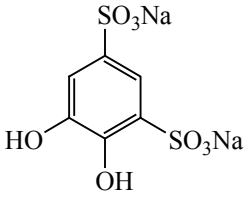

Table 1. Crystallographic data and structure refinement for complexes **1**–**3**

Parameter	Value		
	1	**2**	**3**
Chemical formula	$C_{42}H_{28}N_4O_{24}S_6Tb_2$	$C_{42}H_{28}N_6O_8S_2Fe$	$C_{36}H_{38}N_6O_{13}S_2Fe$
M_r	1482.88	864.67	882.69
Crystal system	Triclinic	Triclinic	Monoclinic
Space group	*P*-1	*P*-1	$P2_1/n$
T, K	296	296	298
a, Å	15.0652(6)	12.879(4)	16.0911(13)
b, Å	20.7059(10)	13.382(4)	13.3631(12)
c, Å	22.1154(9)	14.835(4)	17.9089(15)
α, deg	87.446(1)	104.747(4)	90
β, deg	85.003(1)	100.530(4)	93.231(1)
γ, deg	70.202(1)	107.743(4)	90
V, Å^3	6465.4(5)	2258.8(11)	3844.8(6)
Z	2	2	4
Radiation type	MoK_α	MoK_α	MoK_α
μ, mm^{-1}	1.22	0.48	0.58
Crystal size, mm	0.27 × 0.25 × 0.22	0.27 × 0.25 × 0.22	0.49 × 0.40 × 0.14
Number of reflections [$I > 2\sigma(I)$]			
measured	46922	11991	19163
independent	22619	7910	6756
observed	14384	5285	4118
R_{int}	0.043	0.028	0.073
$(\sin\theta/\lambda)_{max}$, Å^{-1}	0.595	0.595	0.595
$R[F^2 > 2\sigma(F^2)]$	0.069	0.076	0.052
$wR(F^2)$	0.254	0.167	0.117
S	1.11	1.06	1.07
Number of reflections	22619	7910	6756
Number of parameters	691	546	533
Number of restraints	372	84	0
$\Delta\rho_{max}$, $\Delta\rho_{min}$, *e*/Å^3	1.46, –1.29	1.76, –0.88	0.62, –0.37

and two phen moieties (Fig. 1a). Crystallographically, there are two Tb sites with different coordination environments. The Tb^1 ion is eight-coordinated with four phenol oxygen atoms originated from three H_2L^{2-} ligands, two sulfonate oxygen atoms from two H_2L^{2-} ligands as well as two nitrogen atoms of the bidentate chelating phen molecule, while Tb^2 ion is eight-coordinate with five phenol oxygen atoms from three H_2L^{2-} ligands, one sulfonate oxygen atom as well as the bidentate chelating phen molecule. The Tb^1 and Tb^2 atoms reside in distorted double-capped triangular prism and dodecahedral coordination environments, respectively (Fig. 1b). The Tb–O distances are between 2.289(6)–2.432(6) Å, and the Tb–N distances are in the range of 2.506(8)–2.556(6) Å (Table 2), that are comparable with those reported for Tb complexes earlier [19, 20]. The $Tb^1\cdots Tb^2$ distance over three phenol oxygen atoms is 3.561 Å. The Tb^1–O–Tb^2 bond angles are 99.6(2)°, 96.4(2)°, and 97.9(2)° (Table 2). These values are comparable to those reported for Tb complexes [19, 20].

Three unique H_2L^{2-} ligands in complex **1** adopt one type of coordination mode (Fig. 2). Three H_2L^{2-} ligands bridge with two Tb ions via their phenol oxygen and sulfonate oxygen atoms. One phenol group monodentately coordinates with one Tb ion and the other bridges with two Tb ions. All phenol oxygen atoms of H_2L^{2-} ligands are 1*H*-protonated as required for the charge balance. One sulfonate group coordinates with one Tb ion, acting as a monodentate coordination type, whereas the other sulfonate remains non-coordinated and deprotonated.

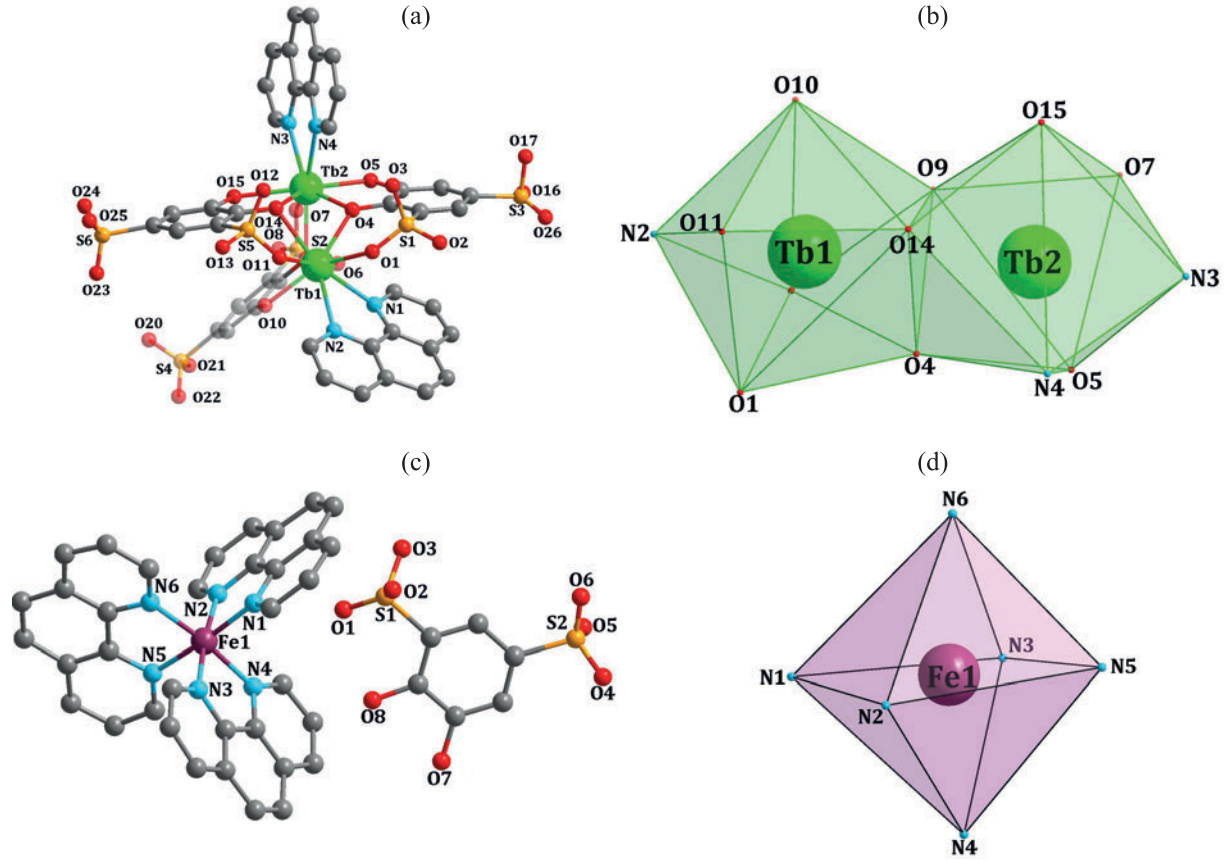

Fig. 1. (a, c) Molecular strutures of complexes **1** and **2** showing the atomic numbering scheme. All H atoms have been omitted for clarity, (b) the coordination configurations of Tb^1 and Tb^2 ions, and (d) Fe^1 ion.

As presented in other references [21], hydrothermal reactions tend to give the 3D coordination polymers with diverse topological structures. When various auxiliary chelating ligands, such as phen and bipy, were used, various types of low dimensional assemblies including mononuclear or dinuclear complexes were formed [22]. The π–π interconnections of two phen moieties between adjacent dinuclear molecules lead to formation of a one-dimensional structure (Fig. 3).

Crystal structures of $Fe(phen)_3 \cdot HL$ (2) and $Fe(bipy)_3 \cdot HL \cdot 5H_2O$ (3). The structures of complexes **2** and **3** are similar, but the ligands containing N-donors. Therefore, the structure of complex **2** is discussed as a sample. Single crystal X-ray diffraction of complex **2** indicates that it crystallizes in the triclinic space group *P*-1 (Table 1). The asymmetric unit consists of one Fe ion, one HL^{3-} anion and three phen species (Fig. 1c). The Fe^1 is six-coordinate and demonstrates an octahedral coordination configuration (Fig. 1d) with the axial positions occupied by two nitrogen atoms (N^2 and N^3) and the equatorial positions occupied by four nitrogen atoms (N^1, N^4, N^5, and N^6). The Fe–N distances range from 1.966(4) to 1.983(4) Å for complex **2**, while the N–Fe–N angles are between 82.65(16)° and 174.16(17)° (Table 2), that are consistent with those determined for the comparable structures [23, 24]. Anion HL^{3-} uncoordinates

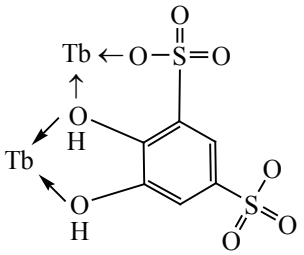

Fig. 2. The coordination mode of H_2L^{2-} ligand.

Table 2. Selected bond lengths and bond angles determined for complexes **1**–**3**

1					
Bond	*d*, Å	Bond	*d*, Å	Bond	*d*, Å
N^{2}–Tb^{1}	2.539(3)	O^{7}–Tb^{2}	2.374(6)	O^{1}–Tb^{1}	2.374(5)
N^{1}–Tb^{1}	2.506(8)	O^{9}–Tb^{2}	2.342(5)	O^{4}–Tb^{1}	2.329(5)
N^{3}–Tb^{2}	2.556(6)	O^{9}–Tb^{1}	2.379(5)	O^{4}–Tb^{2}	2.335(5)
N^{4}–Tb^{2}	2.523(7)	O^{10}–Tb^{1}	2.345(6)	O^{5}–Tb^{2}	2.289(6)
O^{11}–Tb^{1}	2.367(6)	O^{14}–Tb^{1}	2.386(6)	O^{14}–Tb^{2}	2.391(6)
O^{15}–Tb^{2}	2.432(6)				
Angle	φ, deg	Angle	φ, deg	Angle	φ, deg
$O^{4}Tb^{1}O^{10}$	135.46(19)	$O^{5}Tb^{2}O^{4}$	68.5(2)	$O^{4}Tb^{2}N^{3}$	137.1(2)
$O^{4}Tb^{1}O^{11}$	119.2(2)	$O^{5}Tb^{2}O^{9}$	97.8(2)	$O^{9}Tb^{2}N^{3}$	151.3(2)
$O^{10}Tb^{1}O^{11}$	85.1(2)	$O^{4}Tb^{2}O^{9}$	70.26(19)	$O^{7}Tb^{2}N^{3}$	78.1(2)
$O^{4}Tb^{1}O^{1}$	72.30(18)	$O^{5}Tb^{2}O^{7}$	82.4(2)	$O^{14}Tb^{2}N^{3}$	122.5(2)
$O^{10}Tb^{1}O^{1}$	151.68(19)	$O^{4}Tb^{2}O^{7}$	130.2(2)	$O^{15}Tb^{2}N^{3}$	81.2(2)
$O^{11}Tb^{1}O^{1}$	83.2(2)	$O^{9}Tb^{2}O^{7}$	75.08(19)	$N^{4}Tb^{2}N^{3}$	65.0(2)
$O^{4}Tb^{1}O^{9}$	69.72(19)	$O^{5}Tb^{2}O^{14}$	135.0(2)	$O^{10}Tb^{1}N^{2}$	78.73(18)
$O^{10}Tb^{1}O^{9}$	67.42(19)	$O^{4}Tb^{2}O^{14}$	66.8(2)	$O^{11}Tb^{1}N^{2}$	80.20(18)
$O^{11}Tb^{1}O^{9}$	135.7(2)	$O^{9}Tb^{2}O^{14}$	71.12(19)	$O^{1}Tb^{1}N^{2}$	73.90(17)
$O^{1}Tb^{1}O^{9}$	135.71(19)	$O^{7}Tb^{2}O^{14}$	131.8(2)	$O^{9}Tb^{1}N^{2}$	124.09(17)
$O^{4}Tb^{1}O^{14}$	67.0(2)	$O^{5}Tb^{2}O^{15}$	158.2(2)	$O^{14}Tb^{1}N^{2}$	152.13(18)
$O^{10}Tb^{1}O^{14}$	87.7(2)	$O^{4}Tb^{2}O^{15}$	131.0(2)	$N^{1}Tb^{1}N^{2}$	64.19(19)
$O^{11}Tb^{1}O^{14}$	74.4(2)	$O^{9}Tb^{2}O^{15}$	83.0(2)	$O^{7}Tb^{2}N^{4}$	142.0(2)
$O^{1}Tb^{1}O^{14}$	113.65(19)	$O^{7}Tb^{2}O^{15}$	76.8(2)	$O^{14}Tb^{2}N^{4}$	79.1(2)
$O^{9}Tb^{1}O^{14}$	70.58(19)	$O^{14}Tb^{2}O^{15}$	65.96(19)	$O^{15}Tb^{2}N^{4}$	105.0(2)
$O^{4}Tb^{1}N^{1}$	84.0(2)	$O^{5}Tb^{2}N^{4}$	87.6(2)	$O^{5}Tb^{2}N^{3}$	88.4(2)
$O^{10}Tb^{1}N^{1}$	98.2(2)	$O^{4}Tb^{2}N^{4}$	77.9(2)	$O^{14}Tb^{1}N^{1}$	142.7(2)
$O^{11}Tb^{1}N^{1}$	142.6(2)	$O^{9}Tb^{2}N^{4}$	142.8(2)	$O^{4}Tb^{1}N^{2}$	137.96(18)
$O^{1}Tb^{1}N^{1}$	76.4(2)	$O^{9}Tb^{1}N^{1}$	77.8(2)		
2					
Bond	*d*, Å	Bond	*d*, Å	Bond	*d*, Å
Fe^{1}–N^{6}	1.966(4)	Fe^{1}–N^{1}	1.970(4)	Fe^{1}–N^{2}	1.983(4)
Fe^{1}–N^{4}	1.970(4)	Fe^{1}–N^{5}	1.976(4)	Fe^{1}–N^{3}	1.978(4)
Angle	φ, deg	Angle	φ, deg	Angle	φ, deg
$N^{6}Fe^{1}N^{4}$	173.19(18)	$N^{4}Fe^{1}N^{5}$	91.73(17)	$N^{1}Fe^{1}N^{2}$	82.65(16)
$N^{6}Fe^{1}N^{1}$	94.45(17)	$N^{1}Fe^{1}N^{5}$	174.16(17)	$N^{5}Fe^{1}N^{2}$	92.22(16)
$N^{4}Fe^{1}N^{1}$	91.23(17)	$N^{6}Fe^{1}N^{2}$	92.38(17)	$N^{6}Fe^{1}N^{3}$	92.69(16)
$N^{6}Fe^{1}N^{5}$	82.94(17)	$N^{4}Fe^{1}N^{2}$	92.06(17)	$N^{4}Fe^{1}N^{3}$	83.21(17)
$N^{2}Fe^{1}N^{3}$	173.90(17)	$N^{5}Fe^{1}N^{3}$	91.77(16)	$N^{1}Fe^{1}N^{3}$	93.57(16)
3					
Bond	*d*, Å	Bond	*d*, Å	Bond	*d*, Å
Fe^{1}–N^{3}	1.964(3)	Fe^{1}–N^{5}	1.976(3)	Fe^{1}–N^{2}	1.974(3)
Fe^{1}–N^{6}	1.968(3)	Fe^{1}–N^{4}	1.979(3)	Fe^{1}–N^{1}	1.982(3)
Angle	φ, deg	Angle	φ, deg	Angle	φ, deg
$N^{3}Fe^{1}N^{6}$	172.94(11)	$N^{2}Fe^{1}N^{4}$	94.81(11)	$N^{2}Fe^{1}N^{5}$	173.70(11)
$N^{3}Fe^{1}N^{2}$	89.74(11)	$N^{5}Fe^{1}N^{4}$	90.60(11)	$N^{3}Fe^{1}N^{4}$	81.79(12)
$N^{6}Fe^{1}N^{2}$	94.67(12)	$N^{3}Fe^{1}N^{1}$	95.12(12)	$N^{6}Fe^{1}N^{4}$	92.34(11)
$N^{3}Fe^{1}N^{5}$	94.24(12)	$N^{6}Fe^{1}N^{1}$	90.96(11)	$N^{5}Fe^{1}N^{1}$	93.00(12)
$N^{6}Fe^{1}N^{5}$	81.85(12)	$N^{2}Fe^{1}N^{1}$	81.77(12)	$N^{4}Fe^{1}N^{1}$	175.43(11)

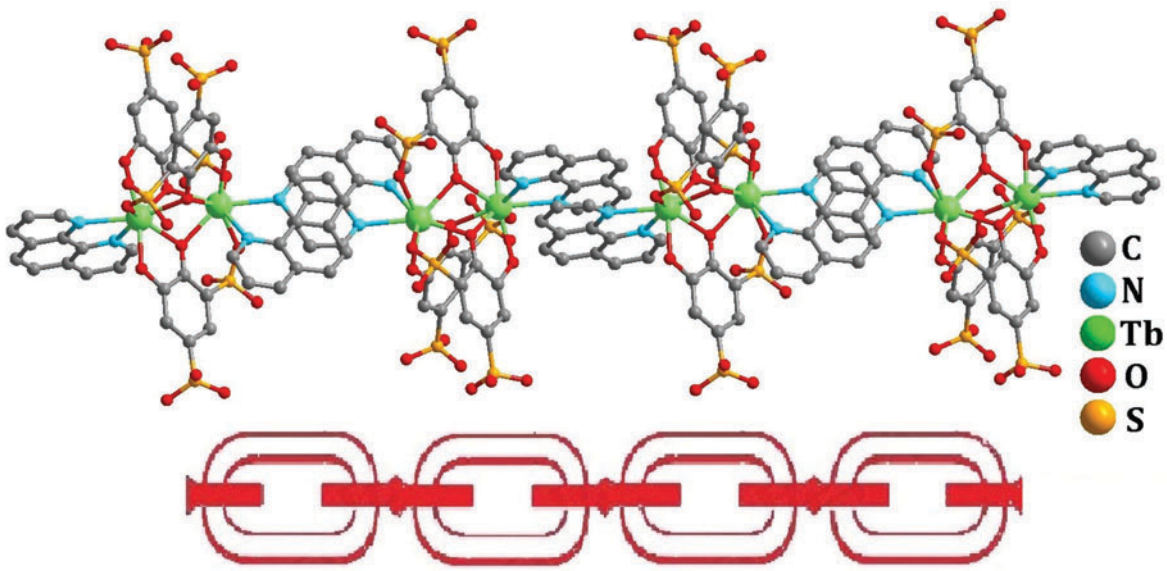

Fig. 3. One-dimensional chain structure composed by the π–π stacting interactions between phen molecules in complex **1**.

with Fe ion, leaving one phenol group 1*H*-protonated for balancing charges.

Thermogravimetric analyses. TGA was performed by heating from 25 to 800°C with the rate of 10°C·min^{-1} under the atmosphere of nitrogen (Fig. 4). For complex **1**, the first weight loss of 5.65% in the range of 25 to 111°C was attributed to the loss of five water molecules (calcd 6.07%). The weight remained constant up to 263°C at which the second weight loss of 24.9% between 263 and 498°C was attributed to the loss of two phen molecules (calcd 24.3%). The skeleton gradually disintegrated between 498 and 624°C. The residue remained stable up to 800°C and consisted of metal sulfate and metal oxide. For complexes **2** and **3**, the initial weight losses of 4.11% and 9.88% were consistent with those of the calculated values (4.16 and 10.20%), corresponding to the loss of two and five water molecules in the temperature ranges of 25–279 and 25–185°C, respectively. In the temperature ranges of 279–367 and 185–337°C the weight losses of 30.57 and 30.86% could take place due to complete decomposition of HL^{3-} anion (calcd 30.92 and 30.27%), respectively. The third weight loss steps indicated decomposition of the phen and bipy molecules in the temperature ranges of 367–800 and 337–800°C,

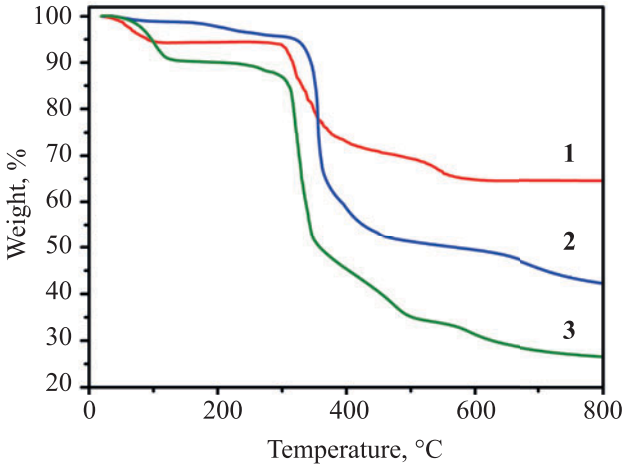

Fig. 4. TGA curves of complexes **1**–**3**.

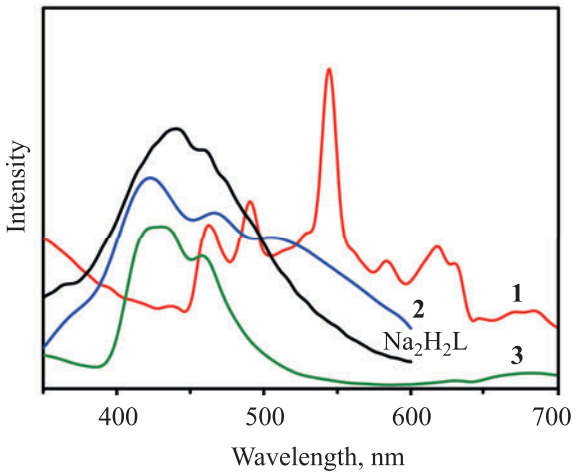

Fig. 5. Solid-state emission spectra of complexes **1**–**3** and free Na_2H_2L ligand at room temperature.

respectively. The residues were the mixtures of metal sulfates and metal oxides, respectively [25].

Luminescence properties. Emission spectra of the complexes **1**–**3** and free Na_2H_2L at room temperature in the solid state were recorded (Fig. 5). For the complex **1**, the dominant peak at 545 nm was hypersensitive, giving green luminescence output, which corresponded to the $^5D_4 \rightarrow {}^7F_5$ transition. Six weak emission peaks at 490, 583, 618, 647, 674, and 705 nm originated from $^5D_4 \rightarrow {}^7F_6$, $^5D_4 \rightarrow {}^7F_4$, $^5D_4 \rightarrow {}^7F_3$, $^5D_4 \rightarrow {}^7F_2$, $^5D_4 \rightarrow {}^7F_1$, and $^5D_4 \rightarrow {}^7F_0$ transitions, respectively [26]. No emission bands from the ligands were observed, indicating that the ligands efficiently transferred the excitation energy to the Tb ions. Emissions observed for complex **1** indicated that it might be potentially applicable as a material for diode devices [27]. Free Na_2H_2L exhibited the maximum fluorescent emission at 440 nm upon excitation at 315 nm, which was attributable to the intraligand π–π* and *n*–π* transitions [28]. Complex **2** exhibited photoluminescent emission with the maximum at 422 nm upon excitation at 315 nm. In the case of complex **3**, a similar photoluminescence with the maximum emission at 430 nm upon excitation at 315 nm was recorded. Peak profiles recorded for complexes **2** and **3** were similar with that of free Na_2H_2L ligand. In addition, those were slightly shifted toward lower wavelengths in comparison with those of free Na_2H_2L ligand indicating that the emission bands of complexes **2** and **3** originated from the intraligand transitions.

EXPERIMENTAL

All chemicals and solvents used in the experiments were of analytical grade, purchased from Sinopharm Chemical Reagent Co., Ltd, and used without further purification. Elemental analyses were carried out after removing water molecules from the samples by heating on an Elementar Vario EL analyzer. Thermogravimentric analyses were carried out on a 1100SF thermal analyzer at the heating rate of 10°C/min under the atmosphere of nitrogen. Photoluminescence analyses were performed on a Perkin Elemer LS55 fluorescence spectrometer.

X-Ray single crystal data were collected for the complexes **1**–**3** on a Bruker Smart Apex II CCD diffractometer equipped with graphite monochromated MoK_α radiation (λ = 0.71073 Å) at 296 and 298 K, respectively. After absorption correction, the structures were solved by the direct method and refined by a full-matrix least squares method on F^2 using SHELXT 2014 and SHELXL 2018 programs [29, 30]. Hydrogen atoms were generated geometrically and treated by a mixture of independent and constrained refinements. The crystallographic data[1] are summarized in Table 1, and the selected bond lengths and angles are presented in Table 2.

Synthesis of $Tb_2(H_2L)_3(phen)_2$ (1). A mixture of $Tb(NO_3)_3 \cdot 6H_2O$(0.045 g, 0.1 mmol) with Na_2H_2L (0.031 g, 0.1 mmol), phen (0.018 g, 0.1 mmol) and deionized water (20 mL) was placed in a Teflon-lined stainless steel autoclave (25 mL) and stirred at room temperature for 1 h. Then the mixture was heated at 120°C for 36 h, followed by cooling down to room temperature. Yellow blocked crystals were collected by filtration. Yield 55% (based on Na_2H_2L). Calculated, %: C 34.02, H 1.69, N 3.78. $C_{42}H_{25}N_4O_{24}S_6Tb_2$. Found, %: C 34.17, H 1.92, N 3.82.

Synthesis of $Fe(phen)_3 \cdot HL$ (2). A mixture of $Fe(NO_3)_3$ (0.024 g, 0.1 mmol) with Na_2H_2L (0.031 g, 0.1 mmol) and phen (0.018 g, 0.1 mmol) in 20 mL of distilled water was stirred at room temperature for 1 h and then stored for 3 days till red blocked crystals were formed. Yield 60% (based on phen). Found, %: C 58.45, H 3.41, N 9.77. $C_{42}H_{28}N_6O_8S_2Fe$. Calculated, %: C 58.33, H 3.24, N 9.72.

Synthesis of $Fe(bipy)_3 \cdot HL \cdot 5H_2O$ (3). Complex **3** was synthesized by the method similar to that of complex **2**. The bipy was used instead of phen. Yield 60% (based on phen). Found, %: C 33.75, H 1.97, N 9.62. $C_{36}H_{38}N_6O_{13}S_2Fe$. Calculated, %: C 48.98, H 4.31, N 9.52.

CONCLUSIONS

In summary, we have reported the syntheses, crystal structures and characterization of three new complexes, namely $Tb_2(H_2Tiron)_3(phen)_2$, $Fe(phen)_3 \cdot HL$, and $Fe(bipy)_3 \cdot HL \cdot 5H_2O$. The N_2H_2L is a multifunctional bridging ligand that can bind to two Tb ions to form a dinuclear complex **1**. One-dimensional supramolecular structure derives from the π–π stacking interactions of the phen ligands in complex **1**. Complexes **2** and **3** have similar N-donor mononuclear structures with

[1] Crystallographic data were deposited with the Cambridge Crystallographic Data Centre (CCDC 2043211, 2043209, 2043210), and can be obtained free of charge via http://www.ccdc.cam.ac.uk/conts/ retrieving. html or from the Cambridge Crystallographic Data Centre, 12 Union Road, Cambridge CB2 1EZ, UK; fax:(+44-1223-336-033; or e-mail: deposit@ccdc.cam.ac.uk).

uncoordinated HL^{3-} anions balancing charges. Their low dimensional structural features depend on the mediation of auxiliary ligands such as phen and bipy. Furthermore, complex **1** shows characteristic emission peaks of Tb^{3+} ions corresponding to $^5D_4 \rightarrow {}^7F_5$, $^5D_4 \rightarrow {}^7F_6$, $^5D_4 \rightarrow {}^7F_4$, $^5D_4 \rightarrow {}^7F_3$, $^5D_4 \rightarrow {}^7F_2$, $^5D_4 \rightarrow {}^7F_1$, and $^5D_4 \rightarrow {}^7F_0$ transitions. Complexes **2** and **3** exhibit the emission bands originated from the intraligand transitions.

FUNDING

Scientific Research Fund Project of Liaoning Provincial Education Department (no. L2019010).

CONFLICT OF INTEREST

No conflict of interests was declared by the authors.

REFERENCES

1. Sougoule, A.-S., Mei, Z.-M., Xiao, X., Balde, C.-A., Samoura, S., Dolo, A., and Zhu, D.-S., *J. Organomet. Chem.*, 2014, vol. 758, p. 19. https://doi.org/10.1016/j.jorganchem.2014.01.034
2. Dey, S., Sarkar, S., Mukherjee, T., Mondal, B., Zangrando, E., Sutter, J.-P., and Chattopadhyay, P., *Inorg. Chim. Acta*, 2011, vol. 376, p. 129. https://doi.org/10.1016/j.ica.2011.06.005
3. Alston, J.-R., Banks, D.-J., Mcneill, C.-X., Mitchell, J.-B., Popov, L.-D., Shcherbakov, I.-N., and Poler, J.-C., *Phys. Chem. Chem. Phys*., 2015, vol. 17, p. 29566. https://doi.org/10.1039/c5cp05419b
4. Guo, Y.-T., Ai, P.-F., Han, L.-Q, Chen, L., Li, B.-G., and Jie, S.-Y., *J. Organomet. Chem.*, 2012, vol. 716, p. 222. https://doi.org/10.1016/j.jorganchem.2012.06.024
5. Suenaga, Y., Nakaguchi, Y., Fujishima, Y., Konaka, H., and Okuda, K., *Inorg. Chem. Commun.*, 2011, vol. 14, p. 440. https://doi.org/10.1016/j.inoche.2010.12.023
6. Yang, H.-X, Guo, S.-P., Tao, J., and Lin, J.-X., *Crystal Growth Des.*, 2009, vol. 9, p. 4735. https://doi.org/10.1021/cg9005983
7. Chartrand, D. and Hanan, G.-S., *Chem. Commun.*, 2008, vol. 53, p. 727. https://doi.org/10.1039/b715205a
8. Maeda, T., Furusho, Y., Shiro, M., and Takata, T., *Chirality*, 2010, vol. 18, p. 691. https://doi.org/10.1002/chir.20308
9. Renz, F., Hill, D., Kerep, P., Klein, M., Müller-Seipel, R., and Werner, F., *Hyperfine Interact.*, 2006, vol. 168, p. 1051. https://doi.org/10.1007/s10751-006-9394-2
10. Xu, G.-H., Tang, B.-B., Hao, L., and Liu, G.-L., *CrystEngComm*, 2017, vol. 19, p. 781. https://doi.org/10.1039/C6CE02292H
11. Kim, J.-Y., Park, I.-H., Lee, J.-Y., Park, J.-M., and Lee, S.-S., *Inorg. Chem.*, 2013, vol. 52, p. 10176. https://doi.org/10.1021/ic401648b
12. Mashima, K. and Nakamura, A., *J. Organomet. Chem*., 2002, vol. 663, p. 5. https://doi.org/10.1016/S0022-328X(02)01728-X
13. Koo, B.-K., Kim, J., and Lee, U., *Inorg. Chim. Acta*, 2010, vol. 363, p. 1760. https://doi.org/10.1016/j.ica.2010.02.032
14. Salehi, M. and Hasanzadeh, M., *Inorg. Chim. Acta*, 2015, vol. 426, p. 6. https://doi.org/10.1016/j.ica.2014.10.023
15. Wang, D.-Z., *J. Molecular Struct.*, 2009, vol. 929, p. 128. https://doi.org/10.1016/j.molstruc.2009.04.013
16. Boghaei, D.-M., Gharagozlou, M., and Sayadi, M., *J. Coord. Chem*., 2007, vol. 60, p. 2283. https://doi.org/10.1080/00958970701261345
17. Chi Y.-X., Niu, S.-Y., Wang, Z.-L., and Jin, J., *Eur. J. Inorg. Chem.*, 2008, vol. 2008, p. 2336. https://doi.org/10.1002/ejic.200800106
18. Wang, D.-Z., *J. Mol. Struct.*, 2009, vol. 929, p. 128. https://doi.org/10.1016/j.molstruc.2009.04.013
19. Aguilà, D., Barrios, L.-A., Luis, F., Repollés, A., and Aromí, G., *Inorg. Chem.*, 2010, vol. 49, p. 6784. https://doi.org/10.1021/ic1008285
20. Yamaguchi, T., Sunatsuki, Y., Ishida, H., Kojima, M., Akashi, H., Re, N., Matsumoto, N., Pochaba, A., and Mroziński, J., *Inorg. Chem.*, 2008, vol. 47, p. 5736. https://doi.org/10.1021/ic8000575
21. Chen, C., Ma, J.-F., Liu, B., Yang, J., and Liu, Y.-Y., *Crystal Growth Des*., 2011, vol. 11, p. 4491. https://doi.org/10.1021/cg2007167
22. Chu, Z.-H., Xie, Q.-F., and Chen, Y.-M., *Chin. J. Inorg. Chem.*, 2013, vol. 29, p. 1893. https://doi.org/10.3969/j.issn.1001-4861.2013.00.222
23. Banse, F., Balland, V., Philouze, C., Riviere, E., and Girerd, J.-J., *Inorg. Chim. Acta*, 2003, vol. 353, p. 223. https://doi.org/10.1016/S0020-1693(03)00292-5
24. Mckeogh, I., Hill, J., Collins, E., McCabe, T., Powell, A., and Schmitt, W., *New J. Chem*., 2007, vol. 31, p. 1882. https://doi.org/10.1039/b711185a
25. Ying, S.-M. and Mao, J.-G., *Eur. J. Inorg. Chem*., 2004, vol. 2004, p. 1270. https://doi.org/10.1002/ejic.200300607
26. Wang, X.-J., Cen, Z.-M., Ni, Q.-L., and Jiang, X.-F., *Crystal Growth Des*., 2010, vol. 10, p. 2960. https://doi.org/10.1021/cg1000045
27. Kariaka, N., Litsis, O., Kolomzarov, Y., Gawryszewska, P., and Amirkhanov, V., *Chem. J. Moldova*, 2018, vol. 13, p. 54. https://doi.org/10.19261/cjm.2018.473
28. Li, S.-N., Zhai, Q.-G., Hu, M.-C., and Jiang, Y.-C., *Z. Anorg. Allg. Chem.*, 2010, vol. 636, p. 1142. https://doi.org/10.1002/zaac.200900450
29. Sheldrick, G.M., *SHELXT-2014*, Program for X-ray Crystal Structure Solution, Göttingen: University of Göttingen, 2014.
30. Sheldrick, G.M., *SHELXL-2018*, Program for X-ray Crystal Structure Refinement, Göttingen: University of Göttingen, 2018.